A sub-10pJ/bit 5Mbps Magnetic Human Body Communication Transceiver

Jiwoong Park, *Student Member, IEEE,* and Patrick P. Mercier, *Senior Member, IEEE*

***Abstract*—This paper presents a transceiver designed to exploit the low path loss offered by magnetic human body communication (mHBC) towards ultra-efficient body-area networking. A single-stage power oscillator is used to efficiently generate on-off-keying (OOK) modulated magnetic fields via body-worn coils that act as both resonant and magnetic-field-generating elements. To de-couple improved path loss yet reduced data rate trade-offs with increasing Q of coils, a synchronous injection-locked kick-start circuit is proposed, enabling 5 Mbps data at a carrier frequency of 40 MHz with a Q of ∼50, while also providing dynamic frequency tuning to compensate normal inductor variation during motion. The receiver exploits the low-path loss towards the design of a low-power sub-threshold-biased dynamic-threshold amplifier and envelope detector, and successfully performs non-coherent demodulation of received OOK data. The transmitter and receiver consume 18.56 and 6.3 μW, which when including a 17.2 μW crystal oscillator for the reference clock, results in an efficiency of 7.15 and 4.7 pJ/bit, respectively when closing a link across the body.**

***Index Terms*—magnetic human body communication, short-range wireless, wireless body-area networks, ultra-low power, energy efficiency, DTMOS.**

I. Introduction

ADVANCES in wearable devices such as wireless headphones, head-mount displays, and medical monitoring sensors have offered exciting opportunities to improve lifestyle in terms of both entertainment and health. Nearly all such wearable devices require wireless communication functionality, either directly to cellular or WiFi access points, or via a local body area network (BAN) which then connects to commodity wireless equipment via a single node (e.g., a smartphone or smartwatch). Since wearable devices must be sufficiently small to comfortably fit within human anatomy, and since radios often dominate the power consumption of such devices [1], ultra-low-power BANs are typically preferred over direct communication to distal access points.

The most popular BAN approach today is Bluetooth Low Energy (BLE). However, this 2.4 GHz RF standard was originally designed for free-space communication at a distance of >10 m, rather than for a short-range BAN: the broadcasting nature of 2.4 GHz RF results in severe loss across the human body, which absorbs RF energy quite well at 2.4 GHz, thereby significantly increasing path loss over free space scenarios [2], [3], as illustrated in Fig. 1(a). As a result, BLE transceivers must support large amounts of power-expensive amplification (e.g., ∼mW-scale for 1 Mbps data transfer), causing BLE to dominate the power of wearable devices, to the point that small devices such as wireless earbuds have battery lives of only a few hours.

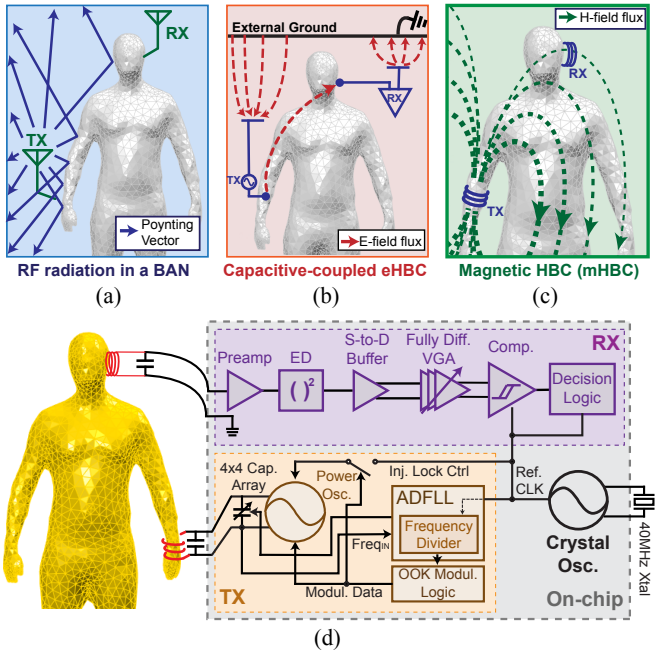

Fig. 1. (a) Conventional RF broadcasting (e.g. Bluetooth). (b) Capacitive electric HBC (eHBC). (c) Magnetic HBC (mHBC). (d) System block diagram of the proposed mHBC transceiver and its high-fidelity audio streaming application

Instead of broadcasting RF energy, researchers have proposed using the human body itself as a conduit for lower-frequency quasi-static fields, as illustrated in 1(b), which theoretically supports lower path loss [4]. Since then, many electric-field-based human body communication (eHBC) transceivers have been demonstrated [5]–[13]. In general, these transceivers have demonstrated improved energy-efficiency over conventional RF approaches due to improved path loss. However, as will described in Section II, path loss measurements were not necessarily done correctly in most cases, with actual losses higher, which will result in reduced energy efficiency in practice. In addition, capacitive coupling to the body and the environment can change substantially with posture and normal movement, which requires bulky dynamically-tunable inductors [14] that are difficult to efficiently implement over a wide range of conditions.

To further reduce path loss and improve the ability to

J. Park and P. P. Mercier are with the Department of Electrical and Computer Engineering, University of California San Diego, La Jolla, CA, 92093, USA (e-mail:pmercier@ucsd.edu). This work was supported in part by the National Science Foundation under Grant No. 1751293.

Manuscript received May 2, 2019.

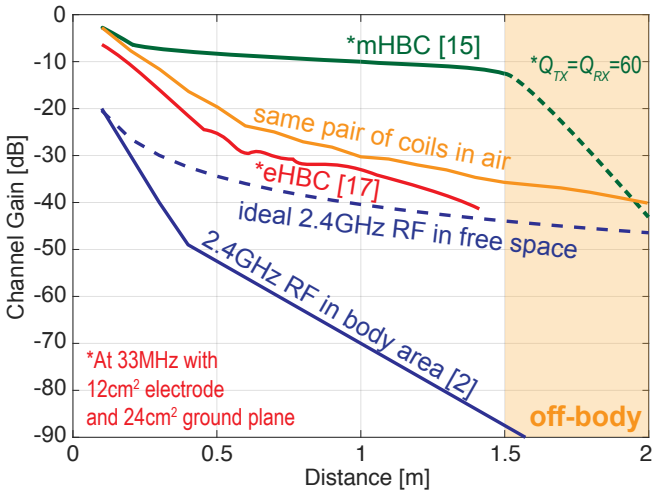

Fig. 2. Channel gain comparison of mHBC to previous wireless BAN approaches.

dynamically tune for varying posture and environmental conditions, we have previously proposed magnetic human body communication (mHBC) [15], illustrated in Fig. 1(c). In mHBC, path loss has been measured to be as low at 10-20 dB across a ∼1 m human body, which compares favorably to ∼80 dB in RF, or ∼40 dB in eHBC. Theoretically, a lower path loss enables the design of transceivers that require less amplification and less complexity, resulting in reduced power consumption towards a longer battery life for wearable devices. Despite demonstrating superior path loss to other solutions, there has not been a transceiver designed to exploit the low path loss of mHBC, beyond the conference paper [16] that this journal paper is based on.

The purpose of this paper is to describe the first mHBC transceiver design in significantly more detail than [16]. We start by briefly describing the mHBC technique in general and contrasting to other BAN approaches in Section II. In Sections III and IV, we discuss how to design a low-power mHBC transmitter (TX) and receiver (RX), respectively, that can each operate at high instantaneous data rates to support high energy efficiency. Section V then reports the performance and specifications of the implemented mHBC transceiver. Finally, in Section VI we verify that the proposed mHBC transceiver works in a practical scenario via the demonstration of 5 Mbps high-fidelity (Hi-Fi) audio data transfer between phone-mounted and ear-mounted prototypes, as illustrated in Fig. 1(d).

II. Wireless Body Area Networking Approaches

A. Sub-6 GHz RF

The most traditional way to communicate across the body involves propagating RF waves operating in one of the main Industrial, Scientific, and Medical (ISM) bands between 400 MHz and 5 GHz. Due to the relatively high conductivity of biological tissues at frequencies in the high-MHz range and beyond, the human body ends up blocking a large fraction of broadcast power from a body-worn antenna, as loosely illustrated in Fig. 1(a). For example, the body shadowing effect increases the 1.5 m channel loss of a 2.4 GHz Bluetooth communication link from 40 dB to upwards of 85 dB [2], as summarized for various BAN-relevant distances in Fig. 2. Another study reported that a 17-cm-long ear-to-ear communication link has 98.2 dB channel loss due to high insertion loss around the brain [3]. Such severe path loss degradation requires higher power communication circuits to achieve higher TX output power as well as better sensitivity and wider dynamic range for RXs. For this reason, researchers have explored other BAN techniques in an attempt to reduce power.

B. eHBC

In 1995, researchers proposed to use the human body as a conduit of quasi-static electric fields [4]. While there are multiple ways to accomplish this, the most popular to date relies on capacitive coupling as illustrated in Fig. 1(b). Many early studies showed that path loss in capacitive eHBC systems could be quite good: for example down 40 dB across the body [17]. However, most such studies did not perform path loss measurements correctly: the presence of large ground planes of measurement and test equipment inadvertently resulted in high-quality capacitive return paths that caused artificially better path loss. In general, the only way to accurately measure eHBC path loss is via battery-powered form-factor-accurate devices [18]. When done in this manner, measurement results reveal worse path loss than previously estimated (e.g., 32 dB over 20 cm at 72 MHz in [18], or 49 dB over 25 cm at <1 MHz in [19]), though still with arguably advantageous performance over far-field RF approaches in a BAN. Figure 2 summarizes the path loss results in [17].

Capacitive eHBC approaches also have favorable multi-user access and security/privacy benefits, since the signals are much more localized to the human body than broadcasting RF. Unfortunately, as a result, capacitive eHBC approaches are also very sensitive to environmental and postural variation. As a capacitive interface, these approaches require a variable inductive matching network, which can be difficult to implement efficiently and reliably over a wide range of conditions [7], [14], [18]. Alternatively, wideband high-impedance termination can be used, which eases variation requirements at the expense of the absence of passive voltage gain [19].

Thus, while there is still promise and potential for eHBC-based BANs, challenges remain. The next subsection will show that mHBC offers additional significant advantages that make it an arguably even more attractive approach.

C. mHBC

Part of the challenge of capacitive eHBC systems is the differential nature of voltage measurements: they require both a sensing and a reference electrode. In capacitive eHBC systems, this configuration means that both the forward and return paths, which are both highly variable, together determine the path loss. In addition, while the human body is conductive, it is not exactly an excellent conductor, which reduces the forward path gain.

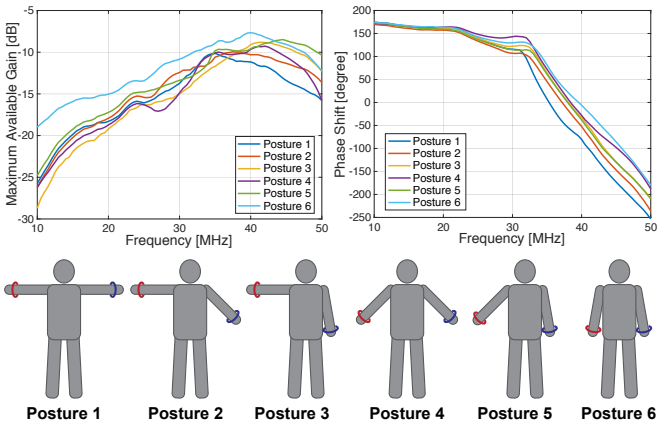

Fig. 3. Measured results of maximum available gain and phase shift of the mHBC channel with various body postures.

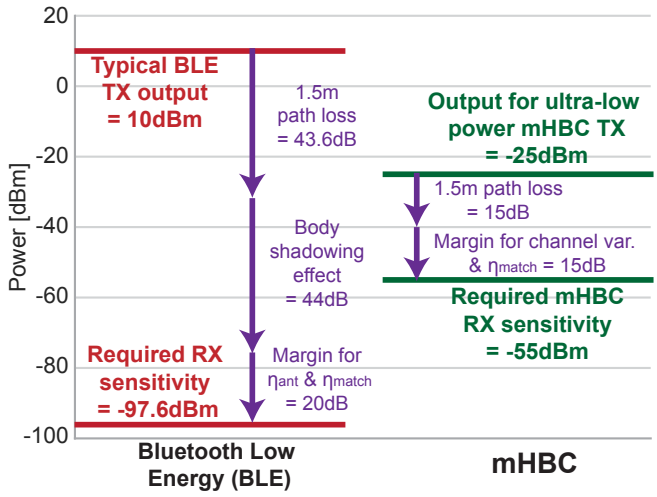

Fig. 4. Comparison of required receiver sensitivity between 2.4 GHz RF Bluetooth Low Energy and mHBC.

The idea for mHBC came from two ideas: the human body is magnetically inert ($\mu_r \approx 1$), and magnetic fields can be sensed in a single-ended manner (i.e., without requiring a reference point), easing implementation requirements and reducing the impact of environmental variation. With $\mu_r \approx 1$ the thought was that magnetic fields should exist within the body just as they would do in air. If mHBC were to operate only in the near field, this conclusion would be correct.

To our surprise, however, the path loss between two coils in both simulations and measurements was actually better with the body in the way at 10s of MHz than when operating in air [15]. Measurement results in air and on the body are summarized in both [15] and Fig. 2. On the body, path loss can be as low as 10 dB, which is far better than RF or eHBC approaches. Due to the inherently single-ended nature, environmental variations are low, and any existing variation can be easily handled by simple capacitive tuning (described in Section III).

While initially surprising, we hypothesize that the improved performance is due the presence of far-field components that have favorable properties at these frequencies on the body. Specifically, it can be briefly noted that due to the high permittivity of biological tissue ($\epsilon_r > 80$), the near-field region boundary ($\lambda/2\pi$) is reduced to 0.13 m in tissue at 40 MHz due to the enhanced far-field radiation which has slower attenuation ($1/r^2$) than the near-field quasi-static ($1/r^6$). It is also known in the literature that magnetic loop antennas (i.e., coils) show better performance than electric dipole antennas in high dielectric dissipative medium such as seawater, which has similar permittivity but higher conductivity than biological tissue [20], [21]. Thus, it can be noted that the proposed mHBC approach, when operating at 10s of MHz across the body, is distinctly different from conventional near-field magnetic approaches, for example Near Field Communication (NFC), or Near Field Magnetic Induction (NFMI), by utilizing components ranging from the near- to the far-field in a similar manner to recent work on mid-field wireless power transfer [22]. With that being said, the far-field contributions and subsequent advantage is currently only a hypothesis, and the exact physics describing mHBC are still under investigation and will be disseminated in a future publication.

Inclusion of far-field components also offer another advantage: less susceptibility to TX-RX misalignment. Figure 3 shows the measured results of maximum available gain (MAG) and the phase shift of an mHBC channel across various different postures, demonstrating reduced path loss variation (i.e., <4 dB across an mHBC channel). Here, the channel gain measurement was performed with a wristband coil pair (Q=60) insulated with thick PVC tube to minimize the effect of capacitive eHBC-like coupling. It can be noted that while path loss experiences very little fluctuation with posture, the phase shift of the mHBC channel does strongly depend on the angle between the two coils. As a result, it is not desirable to employ phase-based modulation schemes in low-power mHBC implementations. Instead, amplitude- or frequency-modulated waveforms are more appropriate. In this work, we employ OOK modulation at 40 MHz.

Due to the extremely good path loss, mHBC offers a significantly relaxed link budget to help reduce required transceiver complexity and power. For example, Fig. 4 illustrated a BLE link budget that, due to the additional 44 dB of body shadowing effect on top of the 43.6 dB path loss across 1.5 m plus margin for matching efficiencies, antenna gain, and so on, requires an RX sensitivity of -97.6 dBm for a 10 dBm TX output power, which requires mW-level power consumption. In contrast, the low mHBC path loss, plus margin for channel variation and matching, permits significantly reduced TX power and sensitivity. Due to fixed overheads in both transmit and receiver circuits, it does not make sense to push TX power too low, or RX noise figure too high, in order to arrive at an optimally-low transceiver power consumption. For example, a -25 dBm TX output power and an -55 dBm RX sensitivity are reasonable link budget selections to enable energy-efficient operation to cover a 1.5 m body-area link. This link budget enables a dramatic reduction in transceiver power consumption, as will described in the following sections.

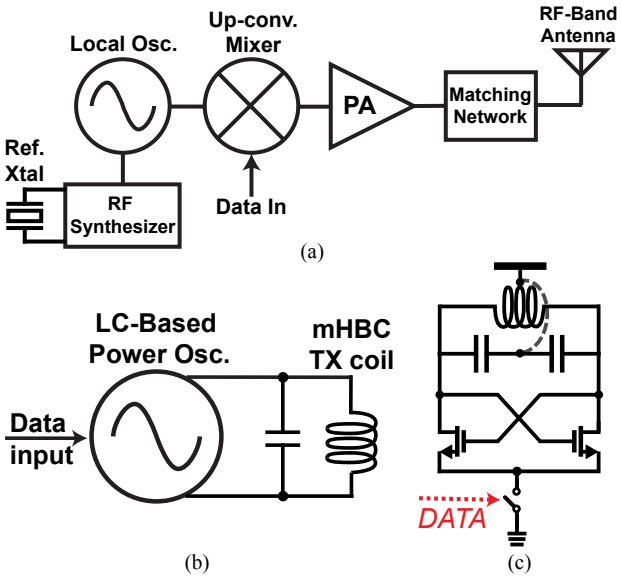

Fig. 5. (a) A generic low-complexity TX architecture often used in low-power wireless BANs. (b) An energy-efficient TX architecture for relatively-low TX output power. (c) A cross-coupled LC oscillator employed for the mHBC TX power oscillator (PO).

III. mHBC Transmitter Implementation

As described in the previous section, the relaxed link budget offered by mHBC affords a very relaxed TX output power specification. Unlike in conventional RF TXs where the output power is so high that the power amplifier largely determines the overall TX efficiency, the power of all downstream components in the TX matters when transmitting such a small amount of power (i.e., -25 dBm is 3 μW), which motivates a simple, low-complexity TX architecture.

Figure 5(a) depicts a conventional TX architecture used in many low-power RF applications. With such a low output power in mHBC, the power overhead of the synthesizer, the mixer, and the power amplifier can be significant, thus deteriorating the global TX efficiency of the architecture [23]. A simpler, lower-overhead approach instead utilizes an inductor as both a radiative and resonant element at RF, as depicted in 5(b) [24], [25]. This architecture is well-suitable for mHBC applications, as a coil is already needed to generate magnetic fields across the body, and can thus be simultaneously repurposed as a resonator in a power oscillator (PO). The general structure of the power oscillator is shown in 5(c), where the tail current source is modulated in order to quench and regenerate the oscillation for on-off-keying (OOK) modulation. Interestingly, capacitively tuning the inductor to the correct frequency enables, in conjunction with the oscillator's positive feedback structure, automatic impedance matching of the coil, and thus no additional matching network is needed.

However, the proposed PO-based TX encounters two principal challenges related to mHBC applications, specifically regarding a trade-off between Q, path loss, and data rate, and frequency stability during motion; both of these will be described in more detail below.

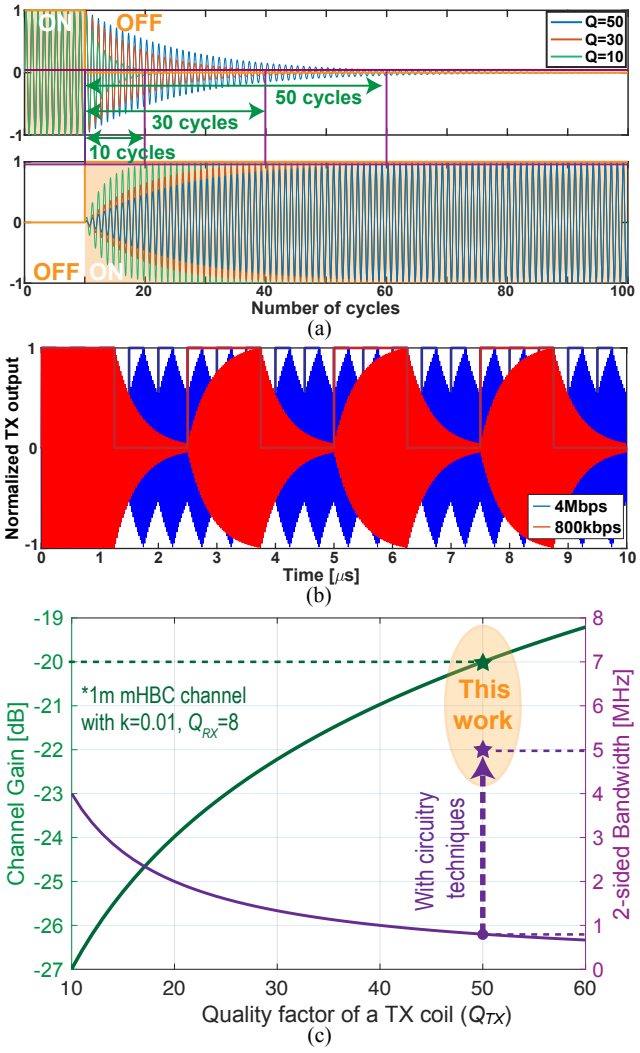

Fig. 6. Illustrating the bandwidth limitation caused by high Q mHBC TX coils: (a) Shut-down and start-up time of the PO, illustrating the need for Q cycles to complete; (b) pushing the data rate too high results in ASK-like modulation with a poor modulation index; and (c) the trade-off between bandwidth and the channel gain.

A. Challenges of PO-based Direct-Modulation Transmitters

1) Bandwidth-path loss trade-off: The achievable 3-dB bandwidth of the transmitter is defined by f_o/Q. This definition implies that Q cycles are nominally required to generate or quench an oscillation to create an OOK symbol. Figure 6(a) illustrates this by showing how long it takes the PO to turn on and off for various Q-factors. Due to this restriction, a Q of 50 at 40 MHz, for example, limits the transmission data rate up to approximately 800 kbps. While faster data rates are technically possible, the oscillator does not have time to settle or quench, resulting in ASK-like modulation with a poor modulation index due to high-Q filtering, as illustrated in Fig. 6 (b). Obviously, reducing the Q of the TX coil can ensure sufficient bandwidth for fast data transmission. However, this Q comes with an important trade-off: path loss of mHBC systems is generally improved with higher Q coils. This trade-off is depicted in Fig. 6 (c), which shows that for the indicated coupling coefficient and Q_{RX}, going from a Q_{TX} of 10 to 50

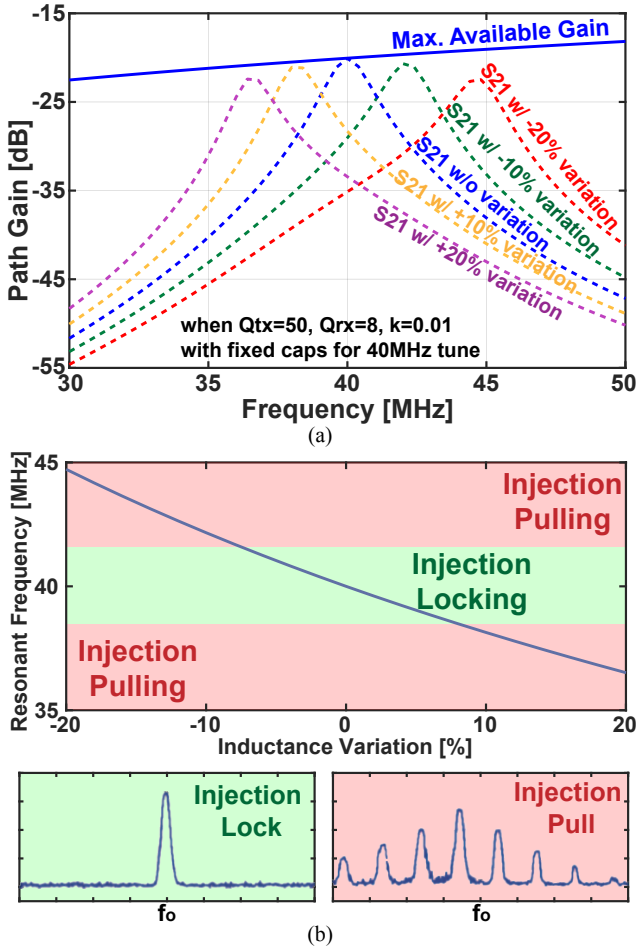

Fig. 7. The inductance fluctuation of wearable mHBC coils: (a) path gain degradation by resonant frequency mismatch between TX and RX; and (b) an example of circuit malfunction: injection pulling.

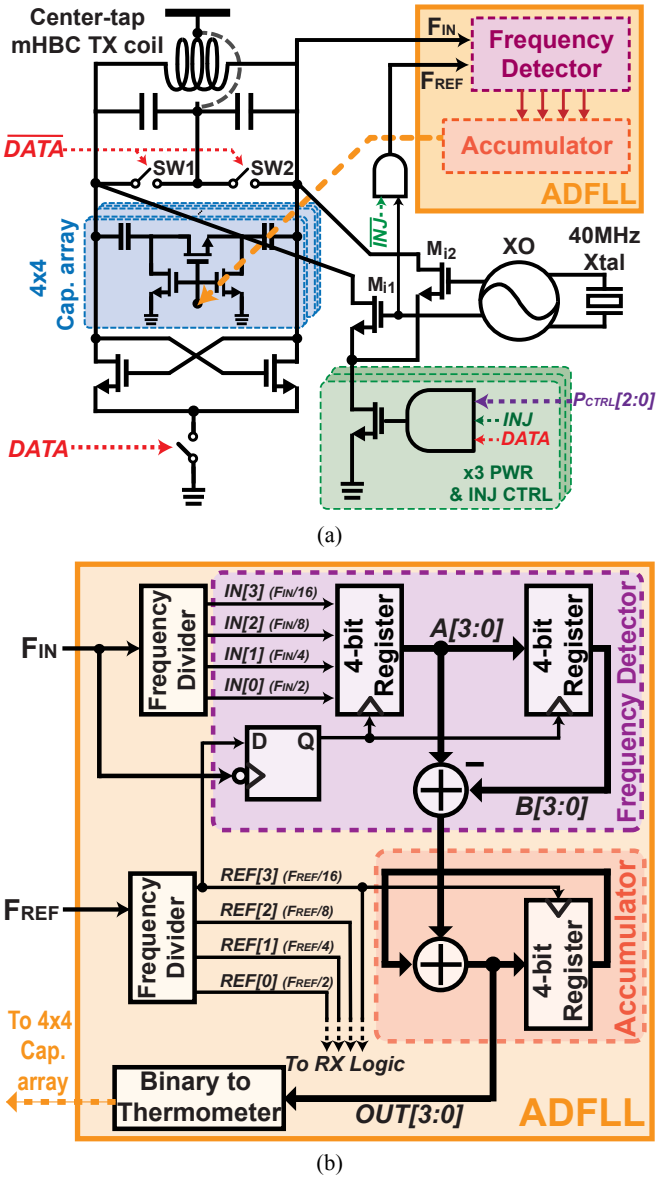

Fig. 8. (a) Proposed TX implementation for fast-data-rate communication and with dynamic resonant frequency calibration. (b) Detailed block diagram of the all-digital-frequency-locked-loop.

improves the path loss by 7 dB. However, at the same time, the bandwidth decreases from 4 MHz to 800 kHz. This trade-off is one of the reasons why conventional NFC protocols utilizing low-frequency (13.56 MHz) near-field coupling cannot support high data rate communications. The specific goal of the TX design is to obviate this trade-off and enable high data rates without sacrificing path loss. Section III-B will describe how this TX design will be accomplished.

2) Inductance variation: It is well known that the inductance of a flexible wearable coil can fluctuate with normal human motion. Although rigid inductors could be used in certain embodiments (e.g., integrated into the housing of a smartphone), their inductance can still vary with environmental variation, albeit less severely than physically flexible coils. Thus, some form of inductance compensation would be useful.

Our experiments indicate that flexible wearable inductors can have inductance variation of up to 20%. Figure 7(a) illustrates how such variation might affect path loss: without compensation, path loss could degrade by up to 15 dB at a carrier frequency of 40 MHz. One possible solution to this is to injection-lock the power oscillator. Figure 7(b) shows that injection locking can help over a $\pm 8\%$ range, but if the resonant frequency of the PO is out of the locking range, the TX output generates harmonic tones that destroy signal fidelity. Fortunately, this inductance variation only occurs at human time scales (milliseconds), and the circuits shown in Sec. III-B will be able to compensate for this variation with more than sufficient speed.

B. TX Circuit Design

Figure 8(a) shows the proposed mHBC TX circuit design to mitigate the challenges and trade-offs described above. The PO consists of a center-tapped mHBC coil, a capacitive DAC for frequency tuning, a cross-coupled pair, and a tail current source used for data modulation. To rapidly kick-start oscillations without having to wait for Q cycles as a conventional implementation would, the PO is injection locked via a 40 MHz crystal oscillator (XO) and transistors M_{i1} and

M_{i2}, which together serve to accelerate oscillator start-up time by 13.3×. Injection power control is enabled via a 3-bit binary weighted current source, enabled only when injection control is enabled and the OOK symbol to be transmitted is a logic "1". To rapidly quench oscillations without having to wait for Q cycles, switches SW1 and SW2 are introduced, which serve to dynamically reduce the tank's Q-factor during off times while improving the quench rate by 10.5×.

In order to ensure the TX is tuned to the correct center frequency, and to further ensure that injection locking is most beneficial, an all-digital frequency-locked-loop (ADFLL) is employed. The fast control bit output (2.5 Moutput/s) of the ADFLL depicted in Fig. 8(b) [26] enables automatic LC oscillation tuning within 10-20 μs, and is only activated between packets every 1-10 ms, which is sufficient to compensate for slow inductance changes (>50-ms scale) of wearable coils.

The proposed rapid kick-start and quenching circuits, along with the ADFLL, help to de-couple the bandwidth-path loss trade-off described above. With the proposed circuitry, the developed mHBC TX successfully generates OOK modulated outputs at 5 Mbps even with a Q of 50 for good path loss, enabling operation in the upper right-hand corner of Fig. 6(c).

IV. mHBC Receiver Implementation

Design of the mHBC receiver must follow similar principals to that of the transmitter: a low-complexity architecture with a small number of blocks is likely preferable. A conventional heterodyne or even a direct-conversion receiver architecture is likely not appropriate, due to the power overhead of LO generation. Instead, most ultra-low-power receiver architectures utilize a direct envelope-detector-based approach [27]–[30]. The following subsection will discuss the typical challenges of such approaches, and how mHBC can help.

A. Design Challenges of Direct-ED Receivers

The most problematic characteristic of direct-ED receivers is that they demodulate everything at their input to baseband - including interferers. Figure 9(a) shows the common-source-amplifier-based (CS-amp-based) ED with an RC low-pass filter implemented in the proposed mHBC RX. Because this ED performs down-conversion utilizing 2nd-order intermodulation harmonics, the conversion gain, $A_{v,conv}$, is determined by the 2nd-order transconductance, g_{m2}, of the employed MOSFET, and the magnitude of the input fundamental carrier tone. Without careful filtering, all broadband interference will be down-converted to baseband, which causes demodulation failure as illustrated in Fig 9(b). To minimize this issue, [28]–[30] implemented high-Q front-end filters to reject interference.

Fortunately, mHBC can alleviate the interference susceptibility thanks to its physically-inherited properties. First of all, an mHBC receiver naturally has a decent bandpass filter via its RX coil. Since there is no easy way to enable wideband data reception at the RX without a priori knowledge of the incoming data, a low-Q coil must be used (noting that the same coil as the TX could be used, but with intentionally de-Q-ing resistors added to the tank). Despite a lower than desired Q (e.g., Q_{RX}=8 here for 5-Mbps data transfer), the

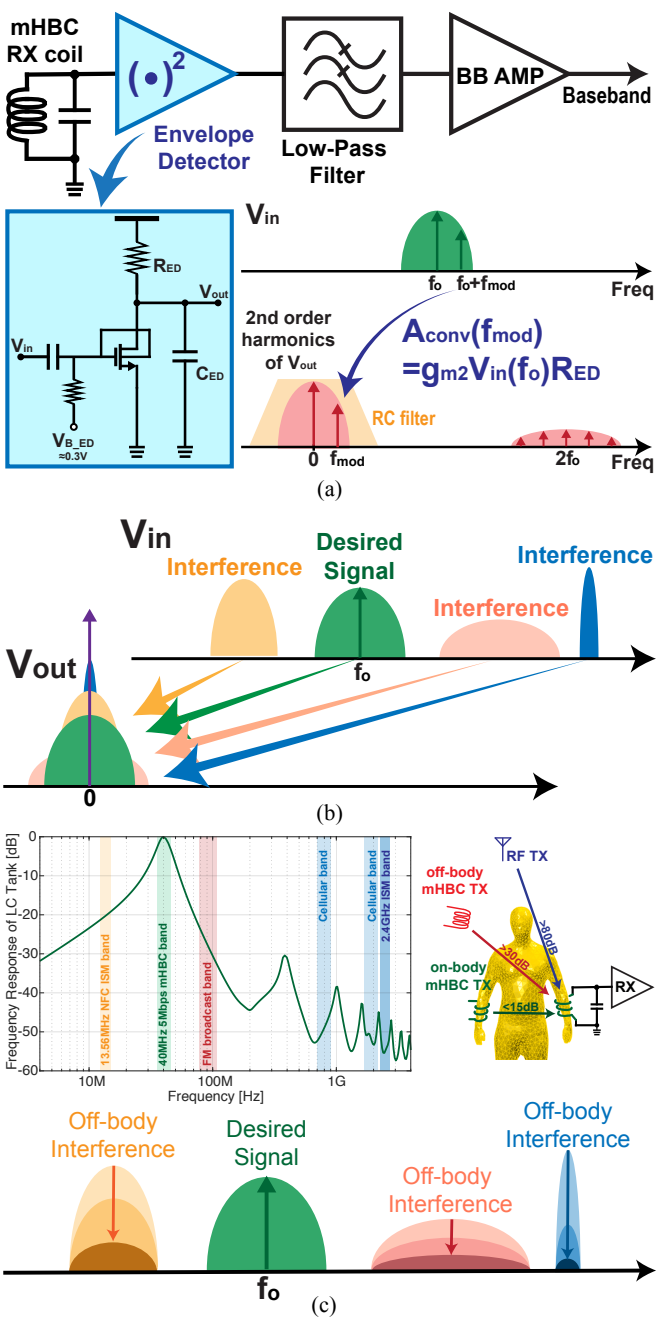

Fig. 9. (a) A CS-amp-based ED with a RC filter and its down-conversion gain by 2nd-order inter-modulation. (b) The interference issue plaguing non-coherent down-conversion receivers without channel selection filters. (c) An additional benefit of mHBC: interference rejection by the RX coil and the human body channel itself.

coil still has the frequency response shown in Fig. 9(c), which shows rejection of interference at the 2.4 GHz ISM band, the FM radio band, and the 13.56 MHz NFC ISM band by up to 56 dB, 33 dB, and 22 dB, respectively. More importantly, the body itself helps to provide additional rejection. As depicted in Fig. 2, RF radios and other off-body magnetic sources (e.g., NFC) have up to 80dB and 25dB more path loss around the body than on-body mHBC, respectively. Therefore, a direct-ED architecture, when used in an mHBC receiver, can tolerate reasonable levels of out-of-band interference, and can thus

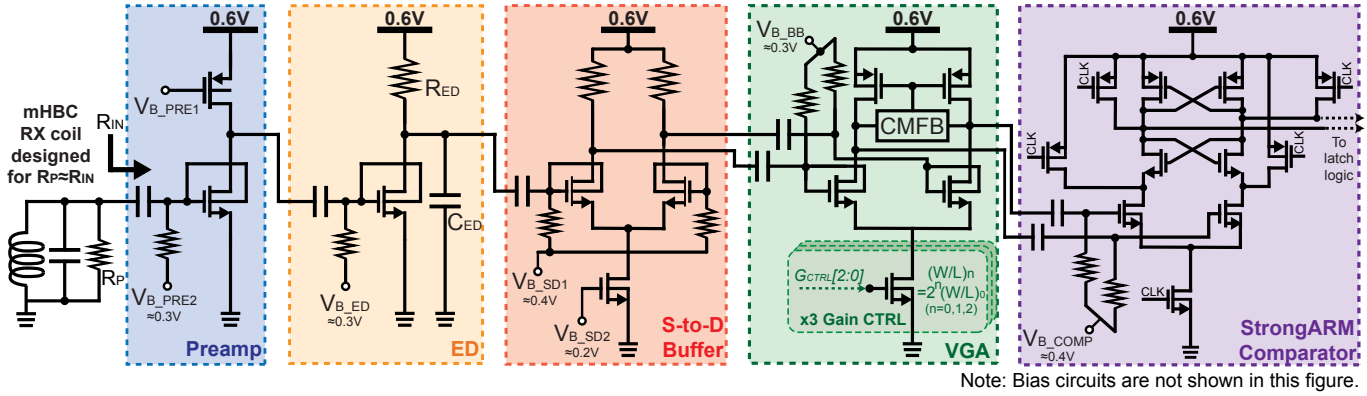

Fig. 10. Proposed ultra-lower power and energy-efficient mHBC RX architecture and its circuit-level design.

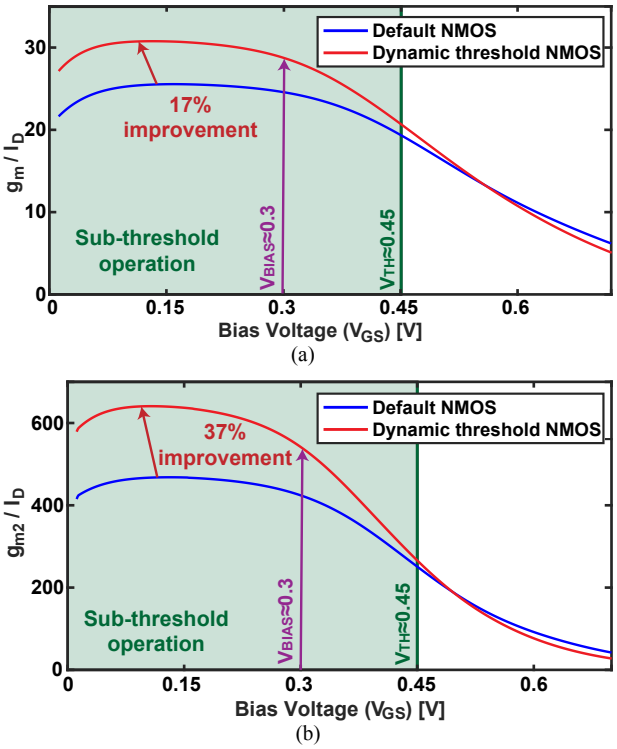

Fig. 11. Improvement of (a) first-order transconductance efficiency and (b) second-order transconductance efficiency of an n-type dynamic-threshold MOSFET in deep sub-threshold operation.

help enable a low-power implementation. Anecdotal testing of the developed receiver in a typical un-shielded lab environment did not show any interference sensitivities. In-band interference, however, can potentially directly degrade the ability to receive the correct signals. While in-band interference is expected to be rare at 40 MHz, a very proximal mHBC user could potentially cause tangible interference. To mitigate this, FDM or TMDA multi-access functionality can be added in future work.

It should also be noted that $A_{v,conv}$ of ED is determined by the voltage magnitude of the fundamental input tone, which can result in poor gain and noise performance depending on the input signal level. For instance, the -55 dBm RX input power of the target RX sensitivity produces a 2 mV input voltage swing with the designed RX mHBC coil. Given a power budget of 3 μW (0.6 V and 5 μA) and R_{ED} of 80 kΩ (for V_{OUT} >100 mV), $A_{v,conv}$ is only 0.443 (-7 dB) and the noise figure (NF) is 55.5 dB, which provides -39.5 dBm RX sensitivity - not good enough. To mitigate this problem, a preamplifier was implemented for better $A_{v,conv}$ and NF, and finally better RX sensitivity. At 40 MHz, the preamplifier power is not exorbitant and is well justified to help improve sensitivity.

B. RX Circuit Design

The overall receiver architecture is shown in Figure 10. As described above, a preamplifier is placed in front of the ED to improve RX sensitivity. The amplifier utilizes an n-type dynamic-threshold MOSFET (DTMOS) for inclusion of g_{mb}. Fig. 11(a) shows that this improves transconductance efficiency (g_m/I_D) by up to 17% when biased into deep subthreshold. The preamplifier was designed to achieve a voltage gain of 19 dB and a noise figure of 31.6 dB, all for 1.8 μW of power consumption. While the noise figure may at first glance sound awful, the power consumption is extremely low and, most importantly, the achieved sensitivity meets the needs of the mHBC link budget, as will described shortly.

The CS-amp-based ED also employs an n-type DTMOS amplifier, in this case, to enhance the 2nd-order transconductance via g_{mb2}, enabling a 37% improved 2nd-order transconductance efficiency (g_{m2}/I_D). By cascading the preamplifier and ED, the down-conversion front-end was designed to achieve $A_{v,conv}$ = 31.1 dB and a noise figure of 35.9dB for 2 mV RX input voltage, which results in -59.1 dBm RX sensitivity with 2.4 μW total power consumption. This RX front-end meets the needs of the proposed mHBC system.

After envelope detection, a single-to-differential (S-to-D) buffer is used to lessen susceptibility to power supply fluctuations and provide low-pass filtering that helps to reject high-frequency harmonics. Here, the S-to-D buffer was designed with low-Vt devices to minimize input capacitance in order to ensure a 2.5 MHz cut-off frequency of the ED RC filter (R_{ED}=400 kΩ and C_{ED}=150 fF). The S-to-D buffer then drives a fully-differential 3-bit variable gain amplifier (VGA). While the VGA compensates the variable noise level of

Chip Summary	
Process	65nm LP
Supply Voltage	0.6V
Carrier Freq.	40MHz
Modulation	OOK
Core Area	0.12mm^2 (TX: 0.02mm^2 RX:0.096mm^2 XO:0.002mm^2)

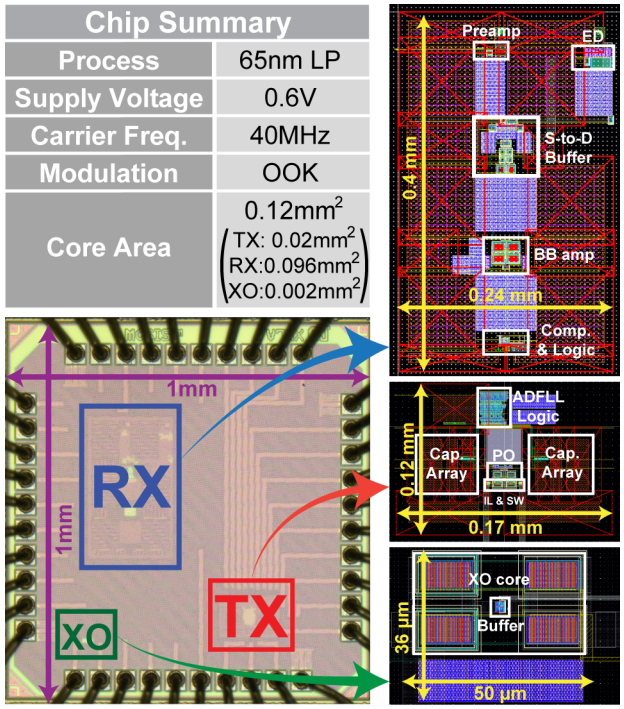

Fig. 12. A implementation summary table, the die photograph, and the layouts of the proposed mHBC transceiver

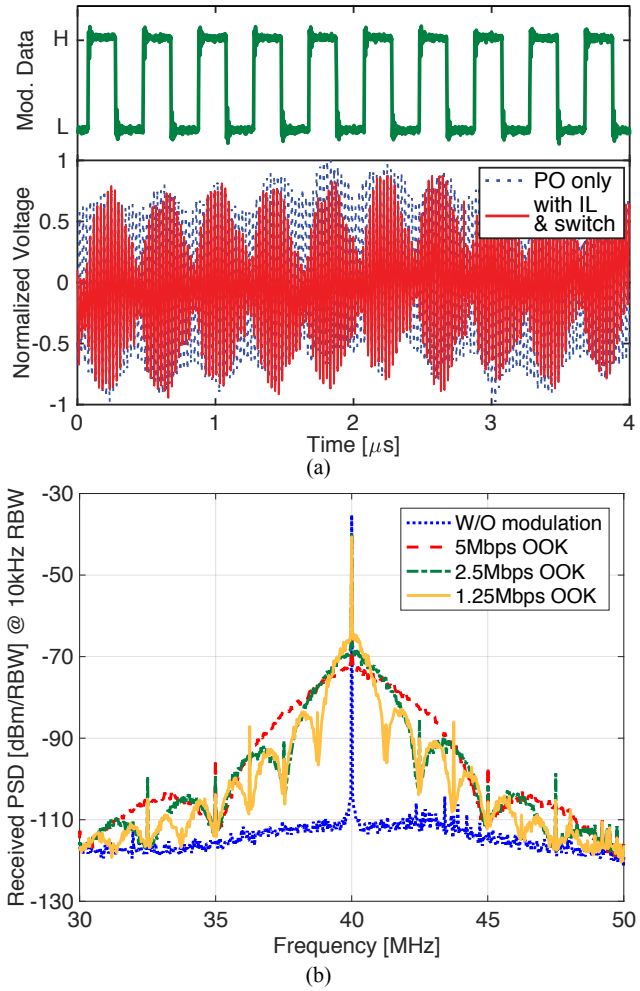

Fig. 13. Measurement results of the high data rate capability of the proposed mHBC TX: (a) 5.5× improved modulation index by rapid-quenching and kick-start circuits; (b) measured OOK modulated spectra with various data rates, received by a wire-wound RX coil (Q_{RX}=8) with 10-cm distance air (12-dB loss).

an ultra-low power comparator, a common-mode feedback (CMFB) circuit adjusts the common-mode voltage of VGA output to the appropriate value to minimize the error of the next-stage comparator. Also, by implementing the oversampling decision scheme in an ultra-low power StrongARM comparator and the following latch logic, the RX architecture can successfully demodulate data without a power-hungry synchronization block. For the better impedance matching performance between the mHBC RX coil and the RX input, the RX coil was designed for the parallel resistance (R_P) at the resonant frequency (40MHz) of the LC tank to have the same resistance value of the RX input.

V. Measurement Results

As summarized in Fig. 12, the mHBC TRX was fabricated in 1×1 mm^2 in 65 nm LP CMOS, and operates with a 0.6 V supply while supporting up to 5 Mbps OOK modulation at 40 MHz with a high-Q (>50) TX coil. The core area of the chip is only 0.12 mm^2 as illustrated by the layouts shown in Fig. 12. The full transceiver requires two external coils, several off-chip shunt tuning capacitors, and a reference crystal. Depending on the power source (e.g., battery voltage), some sort of power management circuits would be needed too (e.g., a 0.6 V LDO).

Figure 13(a) shows the measured TX output waveform under the worst-case modulation that alternates between 1s and 0s at 5 Mbps. With the implementation of the accelerated quenching and oscillation kick-start circuits, the mHBC TX improves the ASK-like modulation index from 15.4% to 84.7%. Figure 13(b) shows OOK spectrum results modulated by externally-applied PRBS bits at data rates of 1.25, 2.5, and 5 Mbps. The signal spectral results were received by an mHBC RX coil across a pre-measured 12-dB-path-loss channel (10 cm distance in air with Q_{TX}=50 and Q_{RX}=8 of the wire-wound wearable coils designed only for test-bench measurements) including bandpass filtering by the RX coil and a narrowband matching network only for the 50 Ω spectrum analyzer input. When de-embedding the filtering of the measurement setup, the main lobe of the modulated TX output is estimated to have a 3-dB bandwidth of 1.24, 2.38, and 4.7 MHz at data rates of 1.25, 2.5, and 5 Mbps, respectively (ignoring the large carrier feedthrough tone due to the lack of phase scrambling).

Figure 14(a) depicts the spectrum and frequency tracking results of dynamic resonant frequency calibration by the ADFLL. Here, to confirm whether the designed ADFLL was working correctly, the LC resonance of the TX PO was intentionally off-tuned to 40.4 MHz (blue dashed line in Fig. 14(a)). Once the FLL starts operating, the capacitor-array DAC in the PO is automatically adjusted to set the oscillation frequency to 40 MHz (green dashed line in Fig. 14(a)) in 10 μs as shown in the measured frequency-tracking result (the

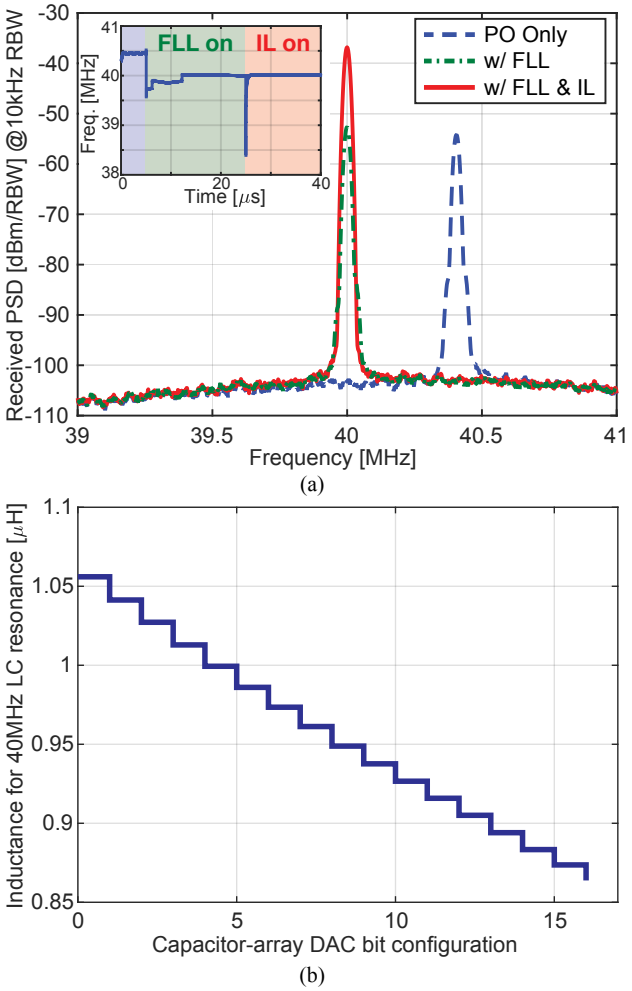

Fig. 14. Measurement results of dynamic resonant frequency calibration for the proposed mHBC TX: (a) measured spectrum and frequency tracking waveform (inset) of ADFLL operation; (b) measured inductance variation coverage by capacitor-array DAC in ADFLL.

inset plot of Fig. 14(a)).

As depicted in Fig. 14(b), the 4×4 capacitor-array DAC with 0.2-pF unit capacitors was designed to cover ±10% inductance variation of a 960-nH mHBC TX coil because a PCB-trace coil for hand-held mHBC applications in Section VI has lower inductance fluctuation ($< \pm 10\%$) than flexible wearable coils. The inductance values for 40 MHz resonance were calculated in Fig. 14(b) with the tuning capacitance (DAC + off-chip fixed capacitors) estimated by the measured resonant frequencies according to the DAC bit configurations and the fixed 960-nH mHBC TX coil.

After a 20 μs calibration period to set the PO resonance frequency in the injection locking range, the injection locking block is turned on to provide the rapid kick-start behavior described in Section III and enhance the TX output power by 17.4dB (red solid line in Fig. 14(a)).

In 3D FEM simulation in Ansys HFSS, a TX output power of -24.8 dBm in the TX default mode causes 73 μW/kg specific absorption rate (SAR), which is much less than the 2 W/kg IEEE regulation. The H-field flux density is 3.2 nT, which is significantly less than an MRI machine (1.5 T), and

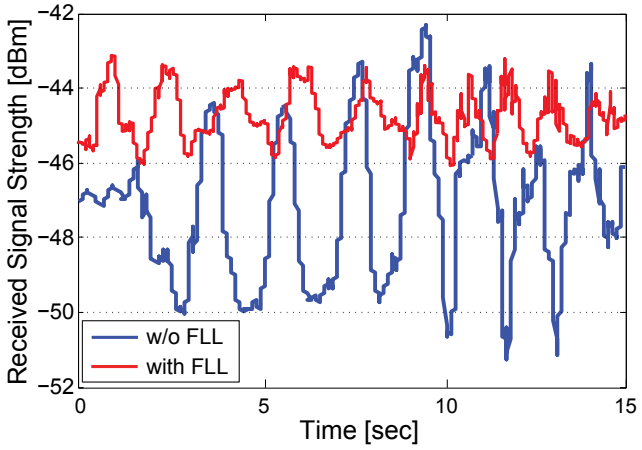

Fig. 15. Measurement results of received signal strength variation under inductance fluctuation by user's moving when the TX output power is -24.8dBm at 40 MHz.

is even less than earth's magnetic field (65 μT).

Figure 15 depicts the received signal strength variation under ordinary walking conditions. Due to both the mis-tuned carrier frequency caused by varying inductance of the TX LC tank and the different channel distance in moving, the received power can be fluctuating by up to 8.9 dB. However, once the ADFLL helps calibrate the resonant frequency to the designed carrier frequency automatically, the received signal strength fluctuates only up to 2.9 dB, which matches the posture data in Fig. 3 well.

Figure 16 shows the RX bit-error-rate (BER) measurement results representing that the 0.1% BER RX sensitivity is -63.5 dBm to -56 dBm at data rates from 1.25 to 5 Mbps, respectively. These BER results were measured by providing the output of a signal generator that has a configurable output impedance to match the RX input (1.8 kΩ). The BER measurements were performed using 2× oversampling decision logic with a clock generated separately by an on-chip XO for asynchronous and non-coherent demodulation conditions. Here, all the curves in Fig. 16 depict the averaged BER curves over ten measurements with arbitrary phase differences between the modulated input signals and the RX logic clock.

Figure 17 demonstrates that a pair of mHBC transceivers with -24.8 dBm TX output power and -56 dBm RX sensitivity settings successfully operated across a human body at 5 Mbps with 388 ns latency (path loss was 20 dB over a 1 m mHBC channel, Q_{TX}=50 and Q_{RX}=8).

As summarized in Fig. 18(a), the mHBC TX transmits -24.8 dBm output power with 18.6 μW of power consumption in the default mode, resulting in an energy efficiency of 3.7 pJ/bit and a TX global efficiency of 9.3%. These TX performance metrics can be improved by changing the TX operation mode (e.g., 1.5 pJ/bit with -34.1 dBm minimum TX output mode, and 13.5% with -22.3 dBm maximum TX output mode). To the authors' knowledge, this is the first wireless BAN transmitter achieving >5% TX global efficiency with <-20 dBm TX output power [23]. With 1.3 pJ/bit energy-efficiency at 6.3 μW of power consumption, the mHBC RX achieves a sensitivity of -56dBm in the default mode and supports a 1.5-m mHBC

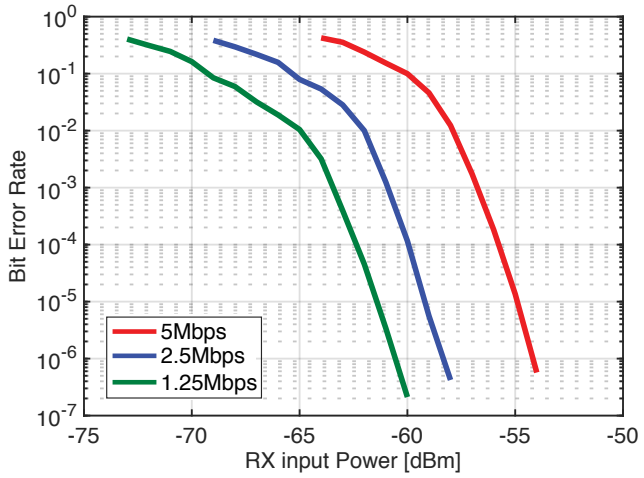

Fig. 16. Measured RX bit-error-rate results with various data rates.

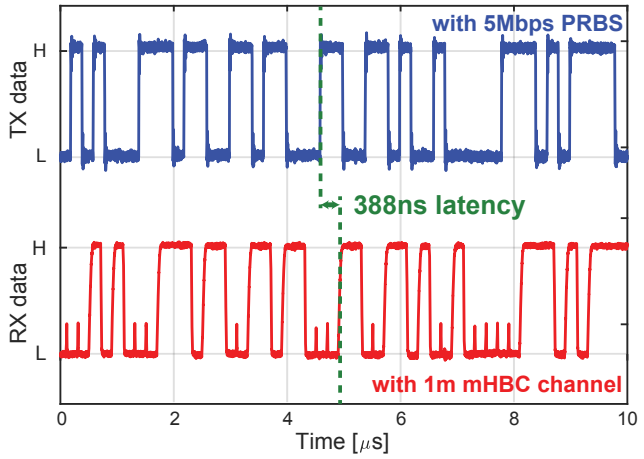

Fig. 17. Measured waveform results of 1-m trans-body TX-to-RX data transfer.

Setting			Min.	Default	Max.
XO	Power [μW]			17.2	
TX (w/ 50% OOK Mod.)	Output power [dBm]		-34.1	-24.8	-22.3
	Power [μW]	PO (with IL)	7.1	18.2	26.0
		ADFLL*		0.02	
		Ctrl Logic		0.34	
		Total	**7.46**	**18.56**	**26.36**
	TX eff. (w/ XO) [%]		**2.7**	**9.3**	**13.5**
	E/bit [pJ/bit]		**1.5**	**3.7**	**5.3**
RX	Sensitivity [dBm] (0.1% BER)		-54	-56	-57
	Power [μW]	Preamp		1.8	
		ED		0.53	
		S-D buffer		2.6	
		BB VGA	0.94	1.3	1.9
		Comp. + Logic		0.07	
		Total	**5.94**	**6.3**	**6.9**
	E/bit [pJ/bit]		**1.2**	**1.3**	**1.4**

*Note : Operates for 20-μs duration every 1 ms.

(a)

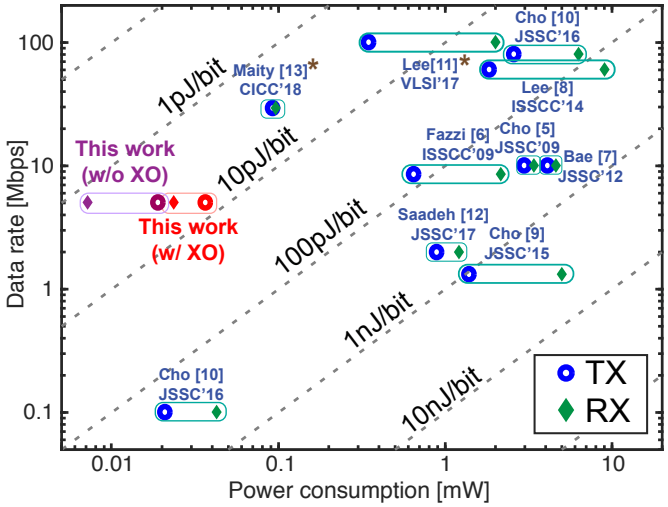

*Note: Not including the power of frequency synthesis.

(b)

Fig. 18. (a) A summary of the proposed mHBC TRX specification. (b) E/bit comparison to the prior eHBC TRXs.

channel using a -24.8 dBm TX output. When including the 17.2 μW from the on-chip XO, the TX and RX consume 35.8 μW (7.15 pJ/bit) and 23.5 μW (4.7 pJ/bit), respectively. This proposed mHBC transceiver is the lowest power and most energy-efficient amongst reported eHBC transceivers when including the energy cost of frequency synthesis as shown in Fig. 18(b) and Table. I.

VI. Demonstration

To demonstrate that the designed mHBC transceiver is capable of operating in a practical wearable application, a Hi-Fi audio data streaming system was developed. As illustrated in Fig. 19(a), 2-channel analog audio data from a smartphone was converted to a 5 Mbps lossless and non-compressed AES3 format, commonly employed in high-performance wired digital audio interfaces, via a 2-channel 24-bit audio ADC and an AES3 encoder.[1] Once the digitized audio data was applied to the mHBC TX data input, the TX generated a 40-MHz 5-Mbps OOK-modulated signal with a 1 mm width 2-turn mHBC TX coil (Q_{TX}=50, L_{TX}=960 nH) printed on the outline of 1-oz copper PCB mounted on the smartphone.

As depicted in Fig. 19(b), the designed TX PCB board contains all the components for audio data transmission, such as an ADC, an AES3 encoder, an mHBC TX, a TX coil, and power management blocks with a coin-cell battery, in the same size as a compact smartphone (11×5.5 cm^2), which mimics when the TX coil is deployed inside the smartphone.

As shown in Fig. 19(c), the mHBC RX unit employed a 32-mm diameter 4-turn wire-wound coil (Q_{RX}=7.6 and L_{RX}=495 nH) mounted inside an in-ear headphone prototype housing while playing the delivered audio data via the AES3 decoder and DAC.

Figure 20 shows that audio data was successfully transmitted from the smartphone TX unit to the headphone RX unit over a 1 m mHBC channel with no error bits and <90 μs

[1]It should be noted that this is not necessarily a pragmatic demonstration - compressed audio is likely a better solution here. However, the main point of this demonstration is to show it is possible to transmit high data rates across the body with high throughput.

TABLE I
PERFORMANCE COMPARISON TABLE

	N. Cho [5] JSSC'09	A. Fazzi [6] ISSCC'09	J. Bae [7] JSSC'12	J. Lee [8] ISSCC'14	H. Cho [9] JSSC'15	H. Cho [10] JSSC'16		J. Lee [11] VLSI'17	W. Saadeh [12] JSSC'17	S. Maity [13] CICC'18	This work
CMOS process	180nm	130nm	180nm	65nm	130nm	65nm		65nm	65nm	65nm	65nm
HBC scheme	eHBC										mHBC
Frequency band [MHz]	30 - 120	1 - 30	40 - 120	40 - 120	18.375 - 23.625	20-60 140-180	13.56	0 - 50	20-120	0 - 15	37.5 - 42.5
Modulation	FSK	Direct Digital	Double FSK	3-level Walsh	BPSK	BPSK	OOK	Direct Digital	P-OFDM BPSK	Direct Digital	OOK
Supply [V]	0.9	1.2	1	1.1	1.2	1.2	0.8	Not Reported	1.1	1	0.6
Maximum data rate	10Mbps	8.5Mbps	10Mbps	60Mbps	1.3125Mbps	80Mbps	100kbps	100Mbps	2Mbps	30Mbps	5Mbps
TX power consumption	2.35mW	0.652mW	3.8mW	1.85mW	1.4mW	2.6mW	21μW	0.35mW†	0.87mW	93μW†	36.7μW
TX E/bit (w/ XO) [pJ/bit]	235	76.7	380	30.8	1067	32.5	210	3.5†	435	3.1†	7.15
RX power consumption	3.7mW	2.15mW	3.2mW	9.02mW	5mW	6.3mW	42.5μW	2mW†	1.1mW	98μW†	23.5μW
RX sensitivity [dBm]	-65	-60	-66	-62	-98.3	-58	-72	Not Reported	-83.1	-63.3	-56.6
RX E/bit (w/ XO) [pJ/bit]	370	253.2	320	150.3	3810	78.8	425	20†	550	3.27†	4.7

† Note: Not including the power of frequency synthesis.

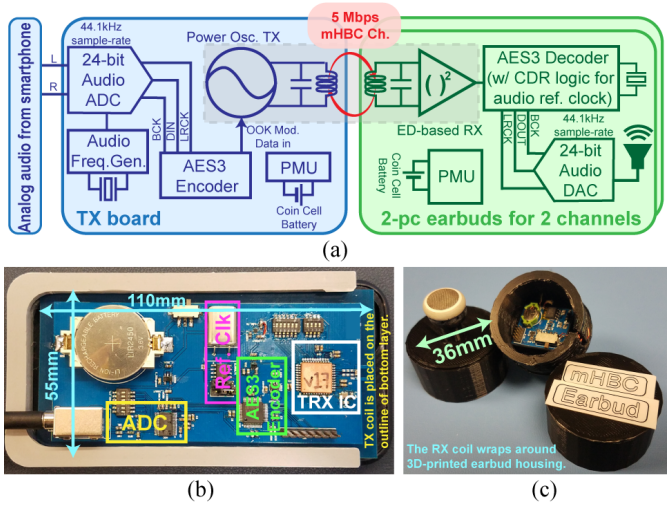

Fig. 19. A Hi-Fi audio streaming demonstration: (a) demonstration block diagram; (b) mHBC TX unit prototype fitted in a compact-sized smartphone; (c) mHBC RX headphone unit prototypes.

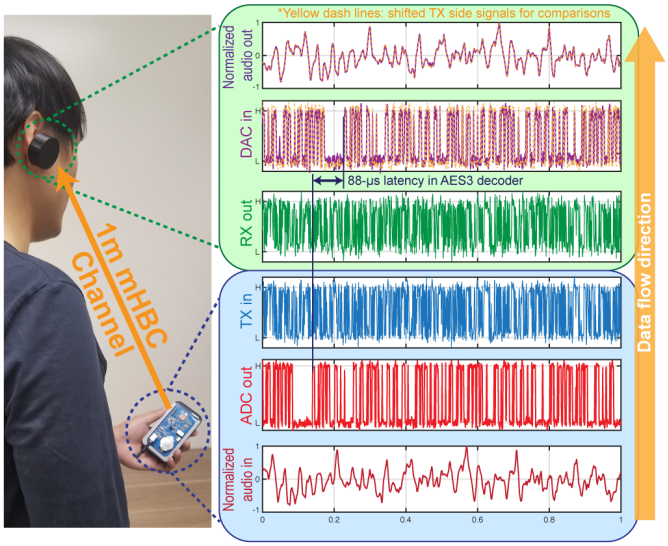

Fig. 20. Waveform results of the proposed mHBC Hi-Fi audio streaming system.

latency (88 μs latency caused by the AES3 decoder), thereby demonstrating that the proposed mHBC transceiver can be used as a real body-area network.

VII. CONCLUSIONS

This paper has presented the first transceiver designed to exploit the low path loss of mHBC communication channels. Implemented in 0.12 mm^2 of core-area in 65 nm, the TX and RX require only 7.15 and 4.7 pJ/bit, respectively, which exceeds the efficiency of prior-art BAN systems that include frequency synthesis by an order of magnitude, all at the lowest demonstrated power consumption when closing a real human body channel link. State-of-the-art efficiency was accomplished by exploiting the inherently low gain of mHBC links to design an ultra-low-power sub-V_{TH} DTMOS-based RX circuits with minimal sensitivity requirements, while employing a direct-PO TX with synchronous kick-start via an ADFLL to raise the data rate when utilizing a high-Q TX coil. A Hi-Fi audio streaming via the designed mHBC transceiver validates the practicality of the promising mHBC scheme.

REFERENCES

[1] P. P. Mercier and A. P. Chandrakasan, *Ultra-Low-Power Short-Range Radios*. New York, NY: Springer, 2015.
[2] P. Hall, Y. Nechayev, A. Alomainy, C. Constantinou, C. Parini, M. Kamarudin, T. Salim, D. Hee, R. Dubrovka, A. Owadally, A. Serra, P. Nepa, M. Gallo, and M. Bozzetti, "Antennas and propagation for on-body communication systems," *IEEE Antennas and Propagation Magazine*, vol. 49, no. 3, pp. 41–58, Jun. 2007.
[3] J. Edelmann and T. Ussmueller, "Can You Hear Me Now?: Challenges and Benefits for Connectivity of Hearing Aids and Implants," *IEEE Microwave Magazine*, vol. 19, no. 7, pp. 30–42, Nov 2018.
[4] T. G. Zimmerman, "Personal Area Networks (PAN): Near-Field Intra-Body Communication," Master's thesis, Massachusetts Institute of Technololgy, Cambridge, MA, 1995.

[5] N. Cho, L. Yan, J. Bae, and H. Yoo, "A 60 kb/s 10 Mb/s Adaptive Frequency Hopping Transceiver for Interference-Resilient Body Channel Communication," *IEEE Journal of Solid-State Circuits*, vol. 44, no. 3, pp. 708–717, March 2009.

[6] A. Fazzi, S. Ouzounov, and J. van den Homberg, "A 2.75mW Wideband Correlation-Based Transceiver for Body-Coupled Communication," in *2009 IEEE International Solid-State Circuits Conference (ISSCC)*, Feb 2009, pp. 204–205.

[7] J. Bae, K. Song, H. Lee, H. Cho, and H. Yoo, "A 0.24-nJ/b Wireless Body-Area-Network Transceiver With Scalable Double-FSK Modulation," *IEEE Journal of Solid-State Circuits*, vol. 47, no. 1, pp. 310–322, Jan 2012.

[8] J. Lee, V. V. Kulkarni, C. K. Ho, J. H. Cheong, P. Li, J. Zhou, W. Da Toh, X. Zhang, Y. Gao, K. W. Cheng, X. Liu, and M. Je, "A 60Mb/s Wideband BCC Transceiver with 150 pJ/b RX and 31 pJ/b TX for Emerging Wearable Applications," in *2014 IEEE International Solid-State Circuits Conference (ISSCC)*, Feb 2014, pp. 498–499.

[9] H. Cho, H. Lee, J. Bae, and H. Yoo, "A 5.2 mW IEEE 802.15.6 HBC Standard Compatible Transceiver With Power Efficient Delay-Locked-Loop Based BPSK Demodulator," *IEEE Journal of Solid-State Circuits*, vol. 50, no. 11, pp. 2549–2559, Nov 2015.

[10] H. Cho, H. Kim, M. Kim, J. Jang, Y. Lee, K. J. Lee, J. Bae, and H. Yoo, "A 79 pJ/b 80 Mb/s Full-Duplex Transceiver and a 42.5 μW 100 kb/s Super-Regenerative Transceiver for Body Channel Communication," *IEEE Journal of Solid-State Circuits*, vol. 51, no. 1, pp. 310–317, Jan 2016.

[11] J. Lee, K. Kim, M. Choi, J. Sim, H. Park, and B. Kim, "A 16.6-pJ/b 150-Mb/s Body Channel Communication Transceiver with Decision Feedback Equalization Improving >200% Area Efficiency," in *2017 Symposium on VLSI Circuits*, June 2017, pp. C62–C63.

[12] W. Saadeh, M. A. B. Altaf, H. Alsuradi, and J. Yoo, "A 1.1-mW Ground Effect-Resilient Body-Coupled Communication Transceiver With Pseudo OFDM for Head and Body Area Network," *IEEE Journal of Solid-State Circuits*, vol. 52, no. 10, pp. 2690–2702, Oct 2017.

[13] S. Maity, B. Chatterjee, G. Chang, and S. Sen, "A 6.3pJ/b 30Mbps 30dB SIR-Tolerant Broadband Interference-Robust Human Body Communication Transceiver Using Time Domain Signal-Interference Separation," in *2018 IEEE Custom Integrated Circuits Conference (CICC)*, April 2018, pp. 1–4.

[14] J. Zhao, J. Mao, T. Zhou, L. Lai, H. Yang, and B. Zhao, "An Auto Loss Compensation System for Non-contact Capacitive Coupled Body Channel Communication," in *2018 IEEE International Symposium on Circuits and Systems (ISCAS)*, May 2018, pp. 1–5.

[15] J. Park and P. P. Mercier, "Magnetic Human Body Communication," in *2015 37th Annual International Conference of the IEEE Engineering in Medicine and Biology Society (EMBC)*. IEEE, Aug. 2015, pp. 1841–1844.

[16] J. Park and P. P. Mercier, "A Sub-40μW 5Mb/s Magnetic Human Body Communication Transceiver Demonstrating Trans-Body Delivery of High-Fidelity Audio to a Wearable In-Ear Headphone," in *2019 IEEE International Solid-State Circuits Conference (ISSCC)*, Feb 2019, pp. 286–287.

[17] J. Bae, H. Cho, K. Song, H. Lee, and H.-J. Yoo, "The Signal Transmission Mechanism on the Surface of Human Body for Body Channel Communication," *IEEE Transactions on Microwave Theory and Techniques*, vol. 60, no. 3, pp. 582–593, Mar. 2012.

[18] J. Park, H. Garudadri, and P. P. Mercier, "Channel Modeling of Miniaturized Battery-Powered Capacitive Human Body Communication Systems," *IEEE Transactions on Biomedical Engineering*, vol. 64, no. 2, pp. 452–462, Feb 2017.

[19] S. Maity, M. He, M. Nath, D. Das, B. Chatterjee, and S. Sen, "BioPhysical Modeling, Characterization and Optimization of Electro-Quasistatic Human Body Communication," *IEEE Transactions on Biomedical Engineering*, pp. 1–1, 2018.

[20] J. R. Wait, "The magnetic dipole antenna immersed in a conducting medium," *Proceedings of the IRE*, vol. 40, no. 10, pp. 1244–1245, Oct 1952.

[21] G. S. Smith, "A theoretical and experimental study of the insulated loop antenna in a dissipative medium," *Radio Science*, vol. 8, no. 7, pp. 711–725, July 1973.

[22] A. S. Y. Poon, S. O'Driscoll, and T. H. Meng, "Optimal frequency for wireless power transmission into dispersive tissue," *IEEE Transactions on Antennas and Propagation*, vol. 58, no. 5, pp. 1739–1750, May 2010.

[23] D. Lee, L. G. Salem, and P. P. Mercier, "Narrowband Transmitters: Ultra low-Power Design," *IEEE Microwave Magazine*, vol. 16, no. 3, pp. 130–142, April 2015.

[24] J. L. Bohorquez, A. P. Chandrakasan, and J. L. Dawson, "A 350 μ W CMOS MSK Transmitter and 400 μW OOK Super-Regenerative Receiver for Medical Implant Communications," *IEEE Journal of Solid-State Circuits*, vol. 44, no. 4, pp. 1248–1259, April 2009.

[25] P. P. Mercier, S. Bandyopadhyay, A. C. Lysaght, K. M. Stankovic, and A. P. Chandrakasan, "A Sub-nW 2.4 GHz Transmitter for Low Data-Rate Sensing Applications," *IEEE Journal of Solid-State Circuits*, vol. 49, no. 7, pp. 1463–1474, July 2014.

[26] V. Kratyuk, P. K. Hanumolu, K. Mayaram, and U. Moon, "A 0.6GHz to 2GHz Digital PLL with Wide Tracking Range," in *2007 IEEE Custom Integrated Circuits Conference*, Sep. 2007, pp. 305–308.

[27] N. E. Roberts, K. Craig, A. Shrivastava, S. N. Wooters, Y. Shakhsheer, B. H. Calhoun, and D. D. Wentzloff, "A 236nW 56.5dBm Sensitivity Bluetooth Low-Energy Wakeup Receiver with Energy Harvesting in 65nm CMOS," in *2016 IEEE International Solid-State Circuits Conference (ISSCC)*, Jan 2016, pp. 450–451.

[28] P. P. Wang, H. Jiang, L. Gao, P. Sen, Y. Kim, G. M. Rebeiz, P. P. Mercier, and D. A. Hall, "A Near-Zero-Power Wake-Up Receiver Achieving 69-dBm Sensitivity," *IEEE Journal of Solid-State Circuits*, vol. 53, no. 6, pp. 1640–1652, June 2018.

[29] A. S. Rekhi and A. Arbabian, "A 14.5mm^2 8nW 59.7dBm Sensitivity Ultrasonic Wake-Up Receiver for Power-, Area-, and Interference-Constrained Applications," in *2018 IEEE International Solid-State Circuits Conference (ISSCC)*, Feb 2018, pp. 454–456.

[30] P. P. Wang and P. P. Mercier, "A 220μW -85dBm Sensitivity BLE-Compliant Wake-Up Receiver Achieving -60dB SIR via Single-Die Multi-Channel FBAR-Based Filtering and a 4-Dimentional Wake-Up Signature," in *2019 IEEE International Solid-State Circuits Conference (ISSCC)*, Feb 2019, pp. 440–442.

Jiwoong Park (S'15) received the B.Sc. degree (summa cum laude) in electronic and computer engineering from Hanyang University, Seoul, Korea, in 2012, and the M.S. degree in electrical and computer engineering from the University of California San Diego (UCSD), La Jolla, CA, USA, in 2014, where he is currently pursuing the Ph.D. degree.

His research interests include the design of ultra-low power body area network systems and the design of miniaturized wireless power transfer systems for biomedical implants.

Patrick P. Mercier (S04−M12−SM17) received the B.Sc. degree in electrical and computer engineering from the University of Alberta, Edmonton,AB, Canada, in 2006, and the S.M. and Ph.D. degrees in electrical engineering and computer science from the Massachusetts Institute of Technology (MIT),Cambridge, MA, USA, in 2008 and 2012, respectively. He is currently an Associate Professor in Electrical and Computer Engineering at the University of California San Diego (UCSD), where he is also the co-Director of the Center for Wearable Sensors. His research interests include the design of energy-efficient microsystems, focusing on the design of RF circuits, power converters, and sensor interfaces for miniaturized systems and biomedical applications.

Prof. Mercier received a Natural Sciences and Engineering Council of Canada (NSERC) Julie Payette fellowship in 2006, NSERC Postgraduate Scholarships in 2007 and 2009, an Intel Ph.D. Fellowship in 2009, the 2009 IEEE International Solid-State Circuits Conference (ISSCC) Jack Kilby Award for Outstanding Student Paper at ISSCC 2010, a Graduate Teaching Award in Electrical and Computer Engineering at UCSD in 2013, the Hellman Fellowship Award in 2014, the Beckman Young Investigator Award in 2015, the DARPA Young Faculty Award in 2015, the UC San Diego Academic Senate Distinguished Teaching Award in 2016, the Biocom Catalyst Award in 2017, and the NSF CAREER Award in 2018. He has served as an Associate Editor of the IEEETRANSACTIONS ON VERY LARGE SCALE INTEGRATION from 2015-2017. Since 2013, he has served as an Associated Editor of the IEEE TRANSACTIONS ON BIOMEDICAL INTEGRATED CIRCUITS, and is currently a member of the ISSCC International Technical Program Committee (Technology Directions Sub-Committee), the CICC Technical Program Committee, the VLSI Symposium Technical Program Committee, and an Associate Editor of the IEEE Solid-State Circuits Letters. Prof. Mercier was the co-editor of Ultra-Low-Power Short Range Radios (Springer, 2015) and Power Management Integrated Circuits (CRC Press, 2016).